Combining Disrupted and Discriminative Topological Properties of Functional Connectivity Networks as Neuroimaging Biomarkers for Accurate Diagnosis of Early Tourette Syndrome Children

Wen, Hongwei; Liu, Yue; Rekik, Islem; Wang, Shengpei; Chen, Zhiqiang; Zhang, Jishui

Published in:
Molecular Neurobiology

DOI:
10.1007/s12035-017-0519-1

Publication date:
2018

Document Version
Peer reviewed version

Combining Disrupted and Discriminative Topological Properties of Functional Connectivity Networks as Neuroimaging Biomarkers for Accurate Diagnosis of Early Tourette Syndrome Children

Hongwei Wen[1,2,3a], Yue Liu[5a], Islem Rekik[7], Shengpei Wang[1,2,3], Zhiqiang Chen[1,2,3], Jishui Zhang[6], Yue Zhang[5], Yun Peng[5*], Huiguang He[1,2,3,4*]

[1] State Key Laboratory of Management and Control for Complex Systems, Institute of Automation, Chinese Academy of Sciences, Beijing, China

[2] Research Center for Brain-inspired Intelligence, Institute of Automation, Chinese Academy of Sciences, Beijing, China

[3] University of Chinese Academy of Sciences, Beijing, China

[4] Center for Excellence in Brain Science and Intelligence Technology, Chinese Academy of Sciences, Beijing, China

[5] Department of Radiology, Beijing Children's Hospital, Capital Medical University, Beijing, China

[6] Department of Neurology, Beijing Children's Hospital, Capital Medical University, Beijing, China

[7] CVIP, Computing, School of Science and Engineering, University of Dundee, UK

[a] These authors contributed equally to this work

[*] Correspondence to:

Huiguang He, State Key Laboratory of Management and Control for Complex Systems, Institute of Automation, Chinese Academy of Sciences, Beijing, 100190, China.

E-mail: huiguang.he@ia.ac.cn

Yun Peng, Department of Radiology, Beijing Children's Hospital, Capital Medical University. No.56 Nanlishi Road, West District, Beijing, 100045, China.

E-mail: ppengyun@yahoo.com

Running Title: Disrupted Functional Networks of TS Children

Abstract

Tourette syndrome (TS) is a childhood-onset neurological disorder. To date, accurate TS diagnosis remains challenging due to its varied clinical expressions and dependency on qualitative description of symptoms. Therefore, identifying accurate and objective neuroimaging biomarkers may help improve early TS diagnosis. As resting-state functional MRI (rs-fMRI) has been demonstrated as a promising neuroimaging tool for TS diagnosis, previous rs-fMRI studies on TS revealed functional connectivity (FC) changes in a few local brain networks or circuits. However, no study explored the disrupted topological organization of whole-brain FC networks in TS children. Meanwhile, very few studies have examined brain functional networks using machine-learning methods for diagnostics. In this study, we construct individual whole-brain, ROI-level FC networks for 29 drug-naive TS children and 37 healthy children. Then, we use graph theory analysis to investigate the topological disruptions between groups. The identified disrupted regions in FC networks not only involved the sensorimotor association regions, but also the visual, default-mode and language areas, all highly related to TS. Furthermore, we propose a novel classification framework based on similarity network fusion (SNF) algorithm, to both diagnose an individual subject and explore the discriminative power of FC network topological properties in distinguishing between TS children and controls. We achieved a high accuracy of 88.79% and the involved discriminative regions for classification were also highly related to TS. Together, both the disrupted topological properties between groups and the discriminative topological features for classification may be considered as comprehensive and helpful neuroimaging biomarkers for assisting the clinical TS diagnosis.

Key words: Tourette syndrome, Children, Functional Connectivity, Graph Theory, Topological Organization, Similarity Network Fusion

Abbreviations: TS = Tourette syndrome, rs-fMRI = resting-state functional magnetic resonance imaging, FC = functional connectivity, DTI = diffusion tensor imaging, WM = white matter, YGTSS = Yale Global Tic Severity Scale, SNF = similarity network fusion

1. Introduction

Tourette syndrome (TS) is a common genetic neurological disorder characterized by the presence of multiple motor and vocal tics. TS commonly begins in childhood, with the typical age of onset between 5 and 7 years [1]. Tics are sudden twitches, movements, or sounds that people do repeatedly. Besides tics, TS is frequently concomitant with other psychiatric comorbidities, mainly obsessive-compulsive disorder (OCD) and other social and behavioral disturbances [2], leading to its heterogeneous clinical expression [3]. The prevalence of TS is now estimated to range between 0.1% and 1% in school-age children with a tendency to increase in recent years [4]. However, since tics are often so mild, especially in childhood, TS are hardly perceived and easily overlooked. To date, TS diagnosis mainly depends on the qualitative description of symptoms, and is still misdiagnosed due to its varied presentation [5] or the interference of other comorbidities. Therefore, developing robust and accurate diagnostic methods is of great importance. Moreover, an early diagnosis of TS would help administer early treatments to the patient, which may help slow down the progression of the disease.

Recently, the non-invasive resting-state functional MRI (rs-fMRI) has emerged as a promising imaging modality for TS studies. Different from structural MRI that reveals brain morphological changes, rs-fMRI can examine spontaneous, low-frequency brain activity in the absence of a task, allowing for studying both functional integration and segregation of brain networks. Existing rs-fMRI studies found significantly altered amplitude of low-frequency fluctuations (ALFF) [6] and regional homogeneity (Reho) [7] in TS patients. However, these studies did not directly measure functional connectivity (FC), which could characterize pairwise correlation between brain regions. Additionally, the biological interpretation of these particular measures is still obscure [8]. More recent studies have implemented a network science approach to investigate functional brain networks in TS. For instance, Church, et al. [9] showed decreased maturity of fronto-parietal and cingulo-opercular cortical networks due to abnormal patterns of connections between functional nodes in pediatric TS patients. Werner, et al. [10] identified abnormal functional connections within the amygdala in TS patients. Worbe, et al. [11] found functional changes in cortico-basal ganglia networks in TS patients, which could reflect a defect in brain maturation. However, these studies only revealed functional changes in a few specific and local networks or circuits, and none of these studies explored the topological organization of whole-brain FC networks. As in recent years, graph theory analysis has become increasingly popular in the neuroimaging and brain network analysis fields, thereby providing advanced tools to investigate the topological organization of brain networks. Functional brain networks exhibit many crucial topological properties, such as small-worldness [12,13] and highly connected hubs [14]. Therefore, it is meaningful to use graph theory analysis for investigating potential disruption in the topological organization of whole-brain FC networks in TS patients, especially in early TS children, which may be an interesting population that offers important insights unravelling the underlying mechanisms of TS.

Furthermore, despite that previous research studies revealed significant functional abnormalities, and advanced our understanding of altered functional networks in TS, those significant abnormalities were identified through comparing patients and controls at group level, which consequently limited clinical translation at the individual level [15]. Therefore, recent attention was turned toward integrating machine-learning and neuroimaging techniques for individualized medicine. On the other hand, unlike group-based comparison approaches, pattern classification based on machine-learning techniques are able to detect the fine-grained spatial discriminative patterns, which are critical for individual-based

disease diagnosis [16]. Indeed, there is a rapidly accumulating evidence that integrating machine-learning and neuroimaging measurements may be valuable for disease diagnosis, transition prediction and treatment prognosis [17].

Although many efforts have been recently made to investigate brain functional or structural networks using machine-learning methods for diagnostics [18-22], only a few were related to TS. For instance, Greene et al. [23] extracted original resting-state functional connectivity (RSFC) as features, then used SVM for TS classification, achieving an accuracy of 74%. Liao et al. [24] extracted original voxel-mirrored homotopic connectivity (VMHC) as features, then used multivariate pattern analysis for TS classification, achieving an accuracy of 92.86%. Wen et al. [25] constructed the structural networks via deterministic tractography, and then the networks were sparsified using a single fixed threshold for subsequent graph theory analysis and TS classification, achieving an accuracy of 88.26%. Nevertheless, these studies have three main drawbacks. Firstly, the two first studies [23,24] extracted the connectivity values as features using the original functional networks, which may have noisy or spurious connections, and should be eliminated via sparsification using proper thresholds. Secondly, no graph theoretical approaches were implemented in these two studies. Since the human brain is a very complex and rich network, solely relying on low-level original connectivity values as features cannot capture high-level topological properties of this network. By contrast, graph theory provides advanced tools to examine the complexity of a network at multiple levels, thus, providing a vast set of objective descriptors of brain structure and function for neuroscientists. Thirdly, though sparsification processing and graph theory analysis were implemented in [25], the selection of a single fixed threshold in this study is subjective and may be affected by different noise levels. Therefore, in this study, we propose a novel classification framework integrating graph theory analysis, a multi-threshold strategy and a network fusion scheme to address the aforementioned limitations.

In the present study, we aim to fully depict the disrupted topological organization of whole-brain FC networks in early TS children, and accurately distinguish TS children from controls using multi-threshold fused network topological features. Briefly, we first use rs-fMRI to construct individual whole-brain, ROI-level FC networks for 29 drug-naive TS children and 37 matched healthy children. Graph theory analysis is then employed to derive the global and regional topological properties. On a group-level, we investigate how TS affects both global/nodal topological properties and the regional distribution of functional hubs. Furthermore, we examine the correlations between these topological changes and the clinical characteristics of TS children. On an individual-level, we use a novel network-based classification framework to accurately distinguish TS children from controls, and identify the discriminative features for classification. Together, both the disrupted (altered) topological properties between groups and the discriminative topological features for classification may be considered as comprehensive and helpful neuroimaging biomarkers for assisting the TS diagnosis.

2. Materials and Methods

2.1 Subjects

29 TS patients were recruited from outpatient clinics in Beijing Children's Hospital from July 2012 to May 2015 (age: 8.76±3.136 years, range: 3–16 years; 6 female). All patients were drug-naive subjects to exclude the effects of stimulants, as previous studies have suggested that stimulants can significantly influence the structure and function of central nervous system in TS [26]. All the patients met

DSM-IV-TR (Diagnostic and Statistical Manual of Mental Disorders, 4th Edition, text revision) criteria for TS. We also included 37 healthy controls in our study (age: 11.19±3.637 years; range: 3–17 years; 12 female). Of note, we have already excluded the participants who have excessive head motion, and the 66 participants were selected after exclusion (see section 2.3). Our research team has professional neurologists and psychiatrists who have gained expertise in diagnosing TS and differentiating it from other complex child mental disorders. The American Psychiatric Association's Diagnostic and Statistical Manual of Mental Disorders, Fifth Edition (DSM-5) was used to help diagnose tic disorders. We used a clinical interview and the Children's Yale-Brown Obsessive Compulsive Scale (CY-BOCS) [27] to diagnose OCD and used the German short version of Wender Utah rating scale (WURS-k, translated to Chinese) [28] to diagnose ADHD. Patients fulfilling ASD (autistic spectrum disorder), OCD, ADHD or other learning disabilities, depression and anxiety criteria were excluded from the study. Tic severity for all patients was rated using the Yale Global Tic Severity Scale (YGTSS) [29] and ranged from 10 to 79 ([mean±SD]: 44.66±17.96). The duration of TS ranged from 3 month to 5 years ([mean±SD]: 1.61±1.38 years). For those who had course less than 1 year, TS diagnosis was made by follow-up call. After the study was approved by Beijing Children's Hospital review board, written informed consent was obtained from all the parents/guardians according to the Declaration of Helsinki. Details of the patients are shown Table 1.

[Insert Table 1 about here]

2.2 Image acquisition

All the participants were scanned using a 3.0 T MR scanner (Gyroscan Interna Nova, Philips, Netherland) at the department of radiology of the Second Affiliated Hospital of Guangzhou University of Traditional Chinese Medicine. The rs-fMRI data were collected using an echo-planar imaging sequence: 30 axial slices; repetition time (TR) = 2000 ms; echo time (TE) = 39 ms; slice thickness = 4 mm; gap = 1 mm; flip angle = 90°; matrix = 64 × 64; field of view (FOV) = 240 mm × 240 mm. During the data acquisition, the participants were asked to lie quietly in the scanner with their eyes closed. After scanning, a total of 180 volumes were obtained for each participant. Individual high-resolution 3D structural images were also acquired using a T1-weighted MP-RAGE sequence: 192 axial slices; TR = 1160 ms; TE = 4.21 ms; inversion time = 600 ms; slice thickness = 0.9 mm; no gap; flip angle = 15°; matrix = 512 × 512; FOV = 256 mm × 256 mm.

2.3 Data preprocessing

Resting-state functional MRI data preprocessing was performed with the SPM8 toolbox. After removal of the first ten volumes, the functional images were corrected for time offsets between slices and geometrical displacements due to head movement. We chose the criteria of 2.0mm and 2.0 degree in max head motion to exclude participants who move excessively. The 29 TS children and 37 healthy children were in fact the selected participants after exclusion. All the corrected functional data were then normalized to the Montreal Neurological Institute space using an optimum 12-parameter affine transformation and non-linear deformations and then resampled to a 3-mm isotropic resolution. Subsequent to smoothing (with FWHM = 8mm), the resulting images were further temporally band-pass filtered (0.01–0.1 Hz) to reduce the effects of low-frequency drift and high-frequency physiological noise, and linear trend was also removed. Finally, several nuisance signals were regressed out from each voxel's time course, including 6-parameter head-motion profiles, global mean signal, mean white matter (WM), and cerebrospinal fluid (CSF) time series within the respective brain

masks derived from prior probability maps (threshold = 0.8) in SPM8 (http://www.fil.ion.ucl.ac.uk/spm).

2.4 Region-based Functional connectivity network

The automated anatomical labeling (AAL) template [30] was used to segment registered fMRI time series into 116 regions, 90 for cortex and 26 for cerebellum (Table 2). For each region, fMRI time series of all voxels lying in that region were averaged to obtain representative fMRI time series or BOLD signal of that region. Then, for each of the 116 ROIs, a mean time series was extracted and Pearson's correlation with all the other ROIs was calculated, therefore outputting a 116×116 correlation matrix. To exclude possible effects of spurious correlations between network nodes, a sparsity threshold (i.e., the ratio of the number of existing edges divided by the maximum possible number of edges in a network) was applied to individual correlation matrices to retain high correlations only. The sparsification approach normalized all resultant networks to have the same number of nodes and edges while minimizing the effects of discrepancies in the overall correlation strength between groups. However, because there is currently no definitive way to select a single threshold, we therefore empirically thresholded each correlation matrix using a wide range of sparsity thresholds [0.08, 0.6] (interval = 0.02) to generate sparse and weighted networks. Figure 1 shows the flowchart of constructing the FC networks of different thresholds.

[Insert Table 2 about here]

[Insert Figure 1 about here]

2.5 Graph Theoretical Approaches

For the resultant networks at each sparsification threshold, we calculated the following network topological attributes. We show the general descriptions for the network properties used in our study in Table 3, as the detailed descriptions were defined in [31,32].

Global network metrics

S_p: network strength (mean degree), E_{glob}: network global efficiency, E_{loc}: network local efficiency, L_p: the shortest path length, C_p: the clustering coefficient, λ: the normalized shortest path length, γ: the normalized clustering coefficient, σ: the small-worldness.

Local nodal characteristics

$B_{nodal}(i)$: nodal betweenness centrality (BC).

[Insert Table 3 about here]

$$B_{nodal}(i) = \sum_{s \neq i \neq t \in G} \frac{e_{st}(i)}{e_{st}} \quad (1)$$

$e_{st}(i)$ denotes the number of shortest paths in the network G between node s and node t, which pass through node i, while e_{st} denotes the total number of shortest paths in the network G between node s and node t. $B_{nodal}(i)$ measures the fraction of all shortest paths that pass through a given node i.

As the global and local topological properties were calculated for each sparsity threshold, similar to

previous studies [33,34], we also calculated the area under the curve (AUC) for each network topological property to provide a summarized scalar independent of single threshold selection [35]. The graph theory analysis in our study was implemented using a MATLAB network analysis toolbox *GRETNA* (Version 1.2, http://www.nitrc.org/projects/gretna/) [36].

2.6 Between-group statistical comparison and correlation analysis

Two-sample t-tests were used to determine the between-group differences in network measure (global and nodal properties). Of note, we used the AUC value of the nodal betweenness centrality across thresholds to analyze nodal properties, including identifying brain hubs and significantly altered nodes. To identify the potential influence of each region on each of the clinical variables, we examined the relationships between the network metrics (global and nodal properties) and each of the clinical variables in the TS group by performing partial correlation analyses using SPSS 19.0 (http://www.ibm.com/analytics/us/en/technology/spss/) (dependent variables: network metrics; independent variables: YGTSS or tics duration; covariates: age and gender).

2.7 Multi-threshold Similarity Network Fusion for subsequent TS classification

To leverage the common and complementary information in multi-threshold networks, we used the similarity network fusion (SNF) algorithm [37] and adapted it to specifically merge the multi-threshold FC networks. The traditional SNF algorithm combined diverse types of genome-wide data to create a comprehensive view of a given disease or a biological process, by constructing networks of samples for each available data (feature) type and then efficiently fusing these into one network that represents the full spectrum of underlying data. In our study, the FC networks with different sparsity thresholds can be considered as diverse feature types. Therefore, the similar ideas can be used to fuse multi-threshold networks to create a comprehensive view of individual FC network for each subject. Briefly, the FC networks of different sparsity thresholds were defined as full kernel matrix W_i^j. For each network W_i^j of subject i with threshold j, a sparse kernel matrix was constructed, which encodes the sparse, strong network connections. Let δ_u denote a set of k-nearest neighbors (the top k strongest connections) of the node u (including u itself) in W_i^j, then the sparse kernel matrix S_i^j is defined as:

$$S_i^j(u,v) = \begin{cases} W_i^j(u,v) & v \in \delta_u \\ 0 & otherwise \end{cases} \quad (2)$$

Where the connection between nodes v and u existed only if v was within the k-nearest neighbors (k=27 in our case) of u. Based on these two kernel matrices, each network could be iteratively updated as follows:

$$(W_i^j)^{(m+1)} = S_i^j \times \frac{\sum_{c \neq j} (W_i^c)^{(m)}}{N-1} \times (S_i^j)^T, c = 1, \quad , N \quad (3)$$

Where $(W_i^c)^m$ denotes the network W_i^c for subject i at the m-th iteration, and $(W_i^j)^{(m+1)}$ represents the updated W_i^j after m+1 iterations. Different thresholded networks provide comprehensive topological views of the original network, W_i^j can integrate the comprehensive information by interacting with all other thresholded networks except itself. Meanwhile, the sparse kernel matrix S_i^j guides the iterative process through the strongest connections of W_i^j, and thus can reduce the noise effectively. From the perspective of matrix multiplication, Eq. (2) implies that the connection of any two nodes in W_i^j also relies on the connections of their neighbors in other thresholded networks. Specially, if the respective

neighbors of two nodes are strongly connected in other thresholded networks, the connection between them can be strengthened after the updates even though it may be weak itself, and vice versa.

The iterative process stops when the fused network remains almost unchanged when updated $\left\|(W_i^j)^{(m+1)} - (W_i^j)^{(m)}\right\| \leq 0.01$. After convergence, we averaged the N networks to obtain the average fused network for subject i:

$$W_i = \frac{\sum_j W_i^j}{N}, j = 1, \quad , N \tag{4}$$

Finally, all elements in W_i were normalized to [0, 1] and the final fused network was obtained for each subject i. Graph theoretical analysis was also performed on the final fused networks, then global properties and nodal betweenness centrality were extracted as features x_i for subject i: $x_i = [S_p, E_{glob}, E_{loc}, L_p, C_p, \lambda, \gamma, \sigma, node_1^{(BC)}, node_2^{(BC)}, ..., node_{116}^{(BC)}]$. The SNF in our study was implemented using a MATLAB toolbox SNFmatlab_v2.1 (http://compbio.cs.toronto.edu/SNF/SNF/Software.html) [37]. The overview of our method is illustrated in Figure 2.

[Insert Figure 2 about here]

2.8 Feature selection and classification

After extracting the features from each individual fused network, we employ a wrapper-based method for feature selection utilizing SVM based on recursive feature elimination which is named SVM-RFE [38]. In this algorithm, SVM is trained iteratively using a selected feature subset. In each iteration, the ranking score for each feature in the selected feature subset is calculated during the SVM training process. The feature with the smallest score is eliminated in each iteration of SVM training until the classification accuracy is over a set threshold, or the number of remaining features in the selected subset is smaller than a set value. Of note, the feature selection was implemented on the training set, rather than entire dataset, using the accuracy of 10-fold cross validation (CV) to estimate the goodness of feature subset, which may avoid the overfitting problem.

Classification was then performed using the SVM algorithm with a radial basis function (RBF) kernel. To estimate optimal values for the two SVM parameters, the complexity or cost constant ($c>0$) and kernel width ($\gamma>0$), we used a grid search in the range of $c=2^{-4}, 2^{-1}, ..., 2^4$ and $\gamma=2^{-8}, 2^{-9}, ...,2^2$, with 10-fold CV to evaluate the goodness of SVM parameters.

In our study, the same nested cross-validation strategy in our previous study [39] was used to evaluate the classification performance. For outer CV, the data is randomly divided into 10 parts in which each class is represented in approximately the same proportions as in the full dataset. Each fold is held out in turn and the learning scheme trained on the remaining nine-tenths and the error rate is then calculated on the tenth fold. Following 10 training procedures, we calculated the average CV accuracy and considered it as the estimation of generalization [40]. The optimal SVM parameters were estimated on the training samples with another 10-fold CV, which is called inner CV. This nested CV strategy can yield an unbiased assessment of the classification method and prevent overestimation. Specifically, this nested CV procedure was repeated twenty times in our study to avoid any bias introduced by randomly partitioning in the cross-validation. Figure 3 shows the flow chart of the evaluation method we used for nested CV.

[Insert Figure 3 about here]

2.9 Evaluation of classification performance

Since our proposed framework had two contributions: (1) graph theory analysis and multiple thresholds processing, and (2) network fusion with SNF, to evaluate its performance, we compared it against three other methods that used:

1. The original FC matrices, without graph theory analysis, 116*115/2 features for each subject.

2. The original FC matrices without sparsity threshold processing, 124 features (8 global and 116 nodal properties) for each subject derived from graph theory analysis.

3. The original FC matrices were sparsified using a single threshold (14%), which was set empirically, 124 features for each subject derived from graph theory analysis.

The same feature selection (SVM-RFE), SVM-based classification, nested CV procedures were then implemented for each of these three comparison methods.

The statistics we used to evaluate our classification algorithm performance are accuracy, sensitivity, specificity and the area under the curve for the receiver operated characteristic curve (AUC ROC). Accuracy is defined as (TP+TN)/(TP+TN+FN+FP) where TP = True Positive, TN =True Negative, FP = False Positive and FN = False Negative. Sensitivity is defined as TP/(TP+FN) and Specificity is defined as TN/(FP+TN).

3. Results

3.1 Alterations in the global properties of FC networks in TS

Both TS patients and normal controls showed a small-world organization of FC networks characterized by $\gamma > 1$ and $\lambda \approx 1$ (Figure 4). However, compared with controls, TS patients had significantly decreased network strength (mean degree), global, local efficiency, clustering coefficient (C_p), and increased shortest path length (L_p), γ, λ and σ in the FC networks over a wide range of thresholds. All the significant p-values (<0.05) were derived after FDR correction [41]. Moreover, TS children showed significantly altered AUC values of all the parameters except λ (Table 4).

[Insert Figure 4 about here]

[Insert Table 4 about here]

3.2 Alterations in the regional properties of FC networks in TS

We investigated between-group differences in regional network measures, specifically nodal betweenness centrality (BC). We considered a node as a hub if its nodal BC is one standard deviation (SD) higher than the average nodal BC of the network. Hubs were quantified for networks based on the AUC of nodal BC curves ($0.08 \leqslant$ sparsity $\leqslant 0.6$, interval = 0.02).

Hub quantification based on AUC analysis revealed that TS and control children showed partially similar hub distributions, with core regions mainly in the right superior frontal gyrus (dorsolateral), parahippocampal gyrus, superior/inferior temporal gyrus, left precentral gyrus, precuneus, dedian cingulate and paracingulate gyri (Table 5, Figure 5A-B). In addition, five hub regions were identified in

the control group only, including the bilateral middle temporal gyrus, left superior frontal gyrus (dorsolateral), right precentral gyrus, dedian cingulate and paracingulate gyri (blue nodes of Figure 5A). Meanwhile, three hub regions were found in TS group only, including the right middle frontal gyrus, precuneus and temporal pole (red nodes of Figure 5B).

[Insert Table 5 about here]

We also compared the AUC values for regional network measure (nodal BC) curves between groups. Compared with healthy children, TS children showed significant altered nodal BC mainly in the superior and inferior frontal gyrus, parietal (angular and inferior parietal gyrus), right occipital (lingual and middle occipital gyrus) and right temporal cortices (fusiform gyrus and hippocampus) (Table 6, Figure 5C). There were no regions in the cerebellum showing significant altered nodal BC. The different colors (red and blue) in Figure 5C indicate the significantly decreased or increased nodal BC in TS group compared with control group. Of note, the regions that showed significantly altered nodal BC between groups were not hub regions except for the right dedian cingulate and paracingulate gyri (DCG) (Figure 5C).

[Insert Table 6 about here]

[Insert Figure 5 about here]

By performing Pearson correlation analysis, we found that the tic severity score (YGTSS) was significantly positively correlated with nodal betweenness centrality of the right parahippocampal gyrus (r=0.496, P=0.006) and left middle temporal gyrus (r=0.371, P=0.047), which were the hubs of TS and control group, respectively. YGTSS was significantly negatively correlated with nodal betweenness centrality of the right inferior frontal gyrus (orbital part) (r=-0.469, P=0.010). In addition, the nodal betweenness centrality of the left heschl's gyrus was significantly positively correlated with both YGTSS (r=0.368, P=0.049) and tic duration (r=0.441, P=0.017) (Figure 6). Of note, we found significantly positive correlation between tics duration and nodal betweenness centrality of the right superior frontal gyrus (dorsolateral) (r=0.402, P=0.031), which is an important hub region in both groups. There were no significant correlations between other network metrics and clinical variables.

[Insert Figure 6 about here]

3.3 **The effects of multi-threshold similarity network fusion algorithm**

To further take insights from our algorithm, we randomly selected three subjects from both groups, respectively. Figure 7 illustrates the original FC networks and the fused networks. Compared to the original networks, our fused networks show more block-like structures with more clear layouts. Besides, the original networks look similar between groups, while the fused networks show significant difference between groups and are relatively similar within each group. The mean connection strength in FC networks of the TS group seems to be weaker than the control group, which perhaps reveals decreased maturity in many specific networks, such as the fronto-parietal and cingulo-opercular cortical networks. Interestingly, this is consistent with the previous TS study [9].

[Insert Figure 7 about here]

3.4 The classification performance of our method

The classification performances of all methods in percentage were showed in Table 7. To exclude the possibility that the classification performance based on one-time randomly partitioning in the CV was not robust and stable, we repeated the nested CV procedure twenty times. Our proposed framework achieved the highest mean (±standard deviation) accuracy (88.79±2.33%), sensitivity (88.45±4.23%), specificity (89.05±3.60%), and AUC (94.96±2.43%), indicating that the high classification power was unlikely the result of chance. Figure 8A plots the receiver operating characteristic (ROC) curves of all methods. Our proposed framework outperforms all 3 comparison methods.

[Insert Table 7 about here]

3.5 Most influential global and nodal properties for Classification

As the highest accuracy was achieved using multi-threshold fused FC networks, the current study also identifies the most discriminative global and nodal topological properties of the fused FC networks for TS classification. We summed the counts of each feature selected by our proposed method over the 20 rounds nested 10-fold CV. The top 29 selected features (5 global and 24 nodal properties) with the frequency more than 50% were provided in Table 8. The most discriminative regions located mainly in the bilateral hippocampus, fusiform gyrus, superior frontal gyrus, rolandic operculum, heschl gyrus, right inferior frontal gyrus (orbital part), putamen and paracentral lobule, left middle frontal gyrus (orbital part), superior frontal gyrus (dorsolateral), caudate nucleus and postcentral gyrus, which may be highly related to TS pathology. Furthermore, the network global, local efficiency, the shortest path length, and the clustering efficiency were also discriminative features. For the purpose of visualization, Figure 8B illustrates the most discriminative regions for classification.

[Insert Table 8 about here]

[Insert Figure 8 about here]

4. Discussion

In the present study, we used rs-fMRI and graph theory to investigate the topological organization of whole-brain, ROI-level FC networks in drug-naive TS children compared with healthy children. Both TS and healthy children showed small-world properties of the FC networks, characterized by high local clustering and short path length. Despite the common small-world topology, TS children showed significantly decreased network strength (mean degree), clustering coefficient, global, local efficiency, and significantly increased shortest path length (L_p). Although both TS and control groups showed partially similar hub distributions, TS children exhibited significant decreased nodal betweenness centrality in multiple functional areas. Furthermore, we proposed a novel network-based classification framework using multi-threshold similarity network fusion algorithm, to distinguish TS children from normal controls, which achieved a high accuracy of 88.79%. The discriminative topological features were also identified. Through combining between-group statistical comparison and individual-based classification, our study may provide empirical evidence for the disrupted topological organization of

FC networks in early TS children.

4.1 Altered Small-world Topology of the FC Networks in TS

Previous studies have proved the small-world property of the brain functional and structural networks constructed using different modal MRI [42-45]. Specially, two previous studies [46,47] showed that functional networks have efficient small-world topological properties in both healthy children and children with attention-deficit hyperactivity disorder (ADHD), a commonly diagnosed childhood neurobehavioral disorders as TS, which could provide certain reference significance for our study.

Although both healthy and TS children showed small-world attributes, the TS children showed significantly decreased network strength, clustering coefficient, global, local efficiency, and significantly increased shortest path length and small-worldness, over a wide range of sparsity thesholds. On one hand, the global efficiency reflects the information transfer between remote cortical regions, and it is mainly associated with long-range connections. On the other hand, the local efficiency is predominantly related to the short-range connections between neighboring regions. Decrease in both global and local efficiencies reflects disrupted topological organizations of the FC networks in TS patients, which seems to be affected by the loss of impaired inter-regional connections as pointed out in [48]. Furthermore, many DTI studies provided direct evidence for disrupted integrity in various WM tracts in early TS children, such as the corticospinal tract, the superior/inferior longitudinal fasciculus, the superior/inferior fronto-occipital fasciculus, the anterior thalamic radiation and the corpus callosum [49,50]. The WM abnormalities may disrupt the inter-regional communication among parts of the brain.

Moreover, significantly decreased clustering coefficient, significantly increased shortest path length and small-worldness were also found over a wide range of sparsity thesholds. Moreover, the AUC value of these parameters also showed the same significance in TS group compared to control group. Increased short path length suggests reduced efficiency of parallel information transfer in the FC networks in TS children. The clustering coefficient represents the ability of a network to process specialized information within densely interconnected groups of nodes (functional segregation). Lower clustering in patients group implies that TS networks are less likely to be connected to each other, thereby indicating that they are less synchronized, segregated and more independent of each other in TS. Since the small-world connectivity model reflects an optimal balance between local specialization and global integration, the significantly altered small-world topology in TS children could indicate less optimal organization of the brain functional networks, possibly as a consequence of reorganization secondary to cortical injury [51].

4.2 Reorganized hub distributions between TS and controls

In this study, we used the nodal betweenness centrality as the key indicator to define the hub regions of brain FC networks. At present, there were no unified standards and methods to define hub regions. Other nodal topological properties such as nodal degree [52] and nodal efficiency [31] were also used to define hub regions in brain network. However, a previous study of resting state functional network [53] used two different nodal topological properties, the nodal betweenness centrality and degree, to find the hubs in brain network respectively. Then vulnerability was employed to compare the two methods, which needs to delete nodes in the network and compare the global efficiency between the intact network and lesioned network. This showed that betweenness centrality was a more effective parameter since the hub's vulnerability of betweenness centrality method was larger than other methods

and the consistency was better. Specifically, betweenness centrality was indeed widely used for hub analysis of brain functional networks [54,14,55], and our study built on these foundations to study the hubs in the FC network.

More importantly, though seven common hub regions were identified in both groups, hub analysis via betweenness centrality in our study demonstrated that partially reorganized hub distributions with three hub regions only appeared in the patient group while five hub regions only appeared in the control groups. Brain hubs with high betweenness centrality were high traffic nodes mediating co-ordination across different functional modules. If the hubs are attacked, the robustness and efficiency of the network will be obviously compromised [56]. Interestingly, the reorganized hubs were all highly related to TS as the local topological properties of these regions were found to be significantly altered in TS children and discriminative for TS classification [25].

4.3 Distributed regions with altered betweenness centrality in TS

We also observed several brain regions with altered nodal betweenness centrality in TS children. The involved regions were categorized into sensorimotor, default-mode, language and visual association functions.

Firstly and importantly, the disrupted regions related to sensorimotor association functions mainly involved the paracentral lobule (PCL), insula and pallidum (PAL). The previous functional imaging studies have observed abnormal neuronal activity in these sensorimotor regions in TS patients. The paracentral lobule controls motor and sensory innervations of the contralateral lower extremity, and its abnormally enhanced structural connectivity with the striatum and thalamus was revealed by a previous study [57], may indicate the significantly increased betweenness centrality of this region. In a previous TS study [58], the insula (mid- and posterior) showed significant resting state FC with bilateral sensorimotor cortex, and the topographic distribution of insula's anatomical connections in primates suggests that it is involved in sensorimotor function. In addition, subthalamic nucleus (STN) neurons in the sensorimotor regions project to the external pallidum, and the left pallidum was found to be positively correlated to tic score [11]. These findings suggest that functional changes exist in the sensorimotor system in TS patients, which provides support for our findings.

Secondly, the disrupted regions in default-mode networks (DMN) mainly involved the hippocampus, inferior parietal lobules (IPL), median cingulate and paracingulate gyri (DCG). Cui et al. [6] found that TS children showed abnormal spontaneous brain activity in cingulate gyrus and parietal gyrus using combined ALFF and fALFF analyses. Hippocampal volume alterations were also found in TS boys and structural changes in hippocampus might indicate an involvement of temporolimbic pathways of the CSTC in the syndrome [59]. Furthermore, the nodal topological properties of DCG were also found to be the discriminative features for TS classification [25]. Above all, the altered betweenness centrality may be due to TS-related disruptions of FC within the DMN and our results are in agreement with these previous findings.

Thirdly, altered nodal BC was observed in several regions that are key components for language processing, which mainly involve the orbital part of inferior frontal gyrus and angular gyrus. The orbital part of inferior frontal gyrus (ORBinf) is most closely represented by Brodmann area (BA) 47, which is implicated in the processing of syntax in oral and sign languages, musical syntax, and semantic aspects of language. Moreover, we observed a significant negative correlation between the nodal betweenness centrality of right ORBinf and the tic severity score of TS children. Interestingly, a previous study [60] also found in TS patients, the YGTSS scores correlated negatively with cortical

thickness in the orbital inferior frontal gyrus (BA 47). The angular gyrus is the part of the brain that is associated with complex language functions, and fMRI activation in angular gyrus were found in TS patients [61]. In this study, 16 of 27 TS patients exhibited vocal tics (including humming, grunting, or saying actual words, usually in an explosive, spastic fashion), which supports our findings of functional abnormalities in the language areas.

Finally, altered nodal betweenness centrality was also found in several occipital regions (MOG and LING) and fusiform gyrus (FFG), which are important for visual processing. Few studies have identified FC abnormalities in the TS patients in the visual regions. Thomalla et al. [62] revealed that TS patients had reduced co-activation in the right MOG, LING and FFG. Wen et al. [50] found that TS children with microstructural abnormalities in the right middle occipital white matter (WM), may indicate a disrupted inter-regional connectivity. Despite these advances, very little is known about the altered topological organization of FC network in the visual regions. Thus, our results provide further evidence for the functional disruption of the visual system in TS patients.

4.4 The benefits of multi-threshold similarity network fusion

From the experimental results, the later three methods in Table 7 based on graph theory outperformed the original FC method without graph theory, and the two methods with sparsity threshold outperformed the method without sparsity threshold. Most importantly, our proposed method based on multi-threshold similarity network fusion has demonstrated a superior performance over other comparison methods. Unlike traditional similarity network fusion [37], which enhances the similar matrix of all samples by integrating different feature types, we further ameliorated the network fusion algorithm to enhance the individual FC network for each subject, by integrating the information provided by other topological views of the original network. The produced fused network does not only rely on a single individual threshold, and thus is less affected by noise. Moreover, it incorporates the common and complementary information from multi-threshold networks, so it can better represent the underlying high-level structure of the original FC network.

4.5 A classification framework with stronger generalization ability to identify neuroimaging biomarkers

In our study, a nested cross-validation strategy was implemented, which might help avoid biased estimates of the classification method and prevent overestimation to a certain extent. In contrast, the previous study [24] used two-sample t-tests on the entire dataset to extract VMHC values showing significant between-group differences, and then used them as features for subsequent classification. Although the classification model was computed based on the training set in their study, the two-sample t-test is in fact a filter methods of feature selection [19], and feature selection on the entire dataset rather than training set, may inadvertently introduce bias into classification models which can result in overfitting. Therefore, the method in their study may cause a model that is enhanced by the selected features over other models being tested to get seemingly better results, when in fact it is a biased result. As a further improvement, we implemented feature selection on the training set, and included the estimations of optimal parameters and model within the inner CV. The nested CV strategy used in our study was considered as the excellent estimation of generalization [40], so the discriminative features identified by our classification framework would be more objective and generalized neuroimaging biomarkers for clinical TS diagnosis.

4.6 Most discriminative features for classification highly related to the pathology of TS

Identification of objective imaging biomarkers is of great interest as it could, ultimately, assist clinical decisions for individual patients. With this consideration, our proposed network-based classification framework identified those topological features that are most discriminative in distinguishing between TS children and controls, thereby identifying brain regions that might be most related to TS. Specifically, many discriminative regions identified by our classification framework were also disrupted regions at the group-level (eg. fusiform gyrus, lingual gyrus, middle occipital gyrus, hippocampus and inferior frontal gyrus, orbital part) or reorganized hub regions (eg. superior frontal gyrus dorsolateral, middle frontal gyrus, superior and middle temporal gyrus). These regions were all highly related to the pathology of TS as previously discussed. Importantly, many global topological properties of the multi-threshold fused networks, such as global, local efficiency, shortest path length and clustering coefficient were also identified as most discriminative features for TS classification. This indicates that the topological organization of FC networks in TS children is affected over a large-scale of sparsity thresholds from another perspective, as the fused networks integrating complementary information from different thresholds.

In addition, our classification framework identified some important regions with discriminative topological features for classification, but showing no significant altered topological properties between groups. These regions were also highly related to the pathology of TS, which mainly involved the bilateral superior parietal gyrus, rolandic operculum, heschl's gyrus, right putamen, left postcentral gyrus, cuneus and caudate nucleus. Superior parietal gyrus as a sensorimotor association region has been found relevant to TS by previous fMRI studies. Buse et al. [63] found decreased prepulse inhibition related BOLD activity in TS boys in the superior parietal cortex. Bohlhalter et al. [64] showed that at the beginning of tic action, significant fMRI activities were found in sensorimotor areas including the bilaterally superior parietal lobule. The rolandic operculum was highly related to tic, as it was found to be commonly activated in free ticcing conditions, by a previous TS study [65] with a variety of fMRI activation paradigms to characterize the origin of tics or their suppression. The basal ganglia have been extensively described in association with TS pathophysiology in children [66,59], especially a functional neuroimaging study has correlated tic occurrence with activity in the putamen and caudate [67]. Moreover, TS patients also had altered FC between left cuneus and bilateral sensorimotor cortex [68] compared to controls, and decreased fractional anisotropy (FA) in the left postcentral WM [50,39] which is also a discriminative region for distinguishing TS children from controls [39], may indicating the TS-related disruptions in these regions.

At present, TS diagnosis largely depends on the qualitative description of symptoms as there is no hallmark imaging abnormality in routine examination or other reliable imaging biomarkers [69,70]. Therefore, our proposed network-based classification framework which exhibited excellent and robust discriminative ability would provide a promising assistance for clinical TS diagnosis. The identified discriminative features were all highly related to the pathology of TS according to previous studies, suggesting that these discriminative topological properties for classification could be reliable neuroimaging biomarkers for clinical TS diagnosis.

5. Conclusion

In our study, we used the whole-brain, ROI-level FC analysis and graph theory analysis to investigate TS-related changes in the topological organization of FC networks. In comparison to healthy controls, we found that, despite TS children showed small-world property, they also showed altered global,

nodal topological properties, and disrupted distribution of hub regions. In particular, the distributed regions not only involved the sensorimotor association regions, but also the visual, default-mode, language areas, all highly related to TS.

Our findings about abnormal functional network properties in TS patients suggested possible neurobiological injuries in specific brain regions that may suffer from fundamentally altered neuronal activity. Furthermore, we proposed a novel network-based classification framework for early TS children identification, using an improved multi-threshold similarity network fusion algorithm especially for FC networks. The experimental results of individual-based diagnosis compared favorably with other diagnositc frameworks. The discriminative network topological features for TS classification were also identified, and the involved brain regions were also highly related to TS. Together, combining the disrupted topological properties between groups and the discriminative topological features for classification, our study may provide potential neuroimaging biomarkers for early-stage TS diagnosis.

Acknowledgements

We thank Dr. Hao Huang at University of Pennsylvania for consultation and support on MR pulse sequences

This work was supported by National Natural Science Foundation of China (61271151, 91520202, 31271161), Youth Innovation Promotion Association CAS and Beijing Municipal Administration of Hospitals Incubating Program (PX2016035)，Beijing health system top level health technical personnel training plan (2015-3-082).

References

1. Lombroso PJ, Scahill L (2008) Tourette syndrome and obsessive–compulsive disorder. Brain and Development 30 (4):231-237

2. Stokes A, Bawden HN, Camfield PR, Backman JE, Dooley JM (1991) Peer Problems in Tourettes Disorder. Pediatrics 87 (6):936-942

3. Cavanna AE, Servo S, Monaco F, Robertson MM (2009) The behavioral spectrum of Gilles de la Tourette syndrome. The Journal of neuropsychiatry and clinical neurosciences 21 (1):13-23. doi:10.1176/appi.neuropsych.21.1.13

10.1176/jnp.2009.21.1.13

4. Scharf JM, Miller LL, Gauvin CA, Alabiso J, Mathews CA, Ben-Shlomo Y (2015) Population prevalence of Tourette syndrome: a systematic review and meta-analysis. Movement disorders : official journal of the Movement Disorder Society 30 (2):221-228. doi:10.1002/mds.26089

5. Cavanna AE, Seri S (2013) Tourette's syndrome. Bmj 347 (2):67-71

6. Cui Y, Jin Z, Chen X, He Y, Liang X, Zheng Y (2014) Abnormal baseline brain activity in drug-naive patients with Tourette syndrome: a resting-state fMRI study. Frontiers in human neuroscience 7:913. doi:10.3389/fnhum.2013.00913

7. Ganos C, Kahl U, Brandt V, Schunke O, Bäumer T, Thomalla G, Roessner V, Haggard P, Münchau A, Kühn S (2014) The neural correlates of tic inhibition in Gilles de la Tourette syndrome. Neuropsychologia 65 (1624):297–301

8. Greene DJ, Schlaggar BL, Black KJ (2015) Neuroimaging in Tourette Syndrome: Research Highlights from 2014 to 2015. Current developmental disorders reports 2 (4):300-308

9. Church JA, Fair DA, Dosenbach NU, Cohen AL, Miezin FM, Petersen SE, Schlaggar BL (2009) Control

networks in paediatric Tourette syndrome show immature and anomalous patterns of functional connectivity. Brain 132 (Pt 1):225-238. doi:10.1093/brain/awn223
10. Werner CJ, Stocker T, Kellermann T, Wegener HP, Schneider F, Shah NJ, Neuner I (2010) Altered amygdala functional connectivity in adult Tourette's syndrome. European archives of psychiatry and clinical neuroscience 260 Suppl 2:S95-99. doi:10.1007/s00406-010-0161-7
11. Worbe Y, Malherbe C, Hartmann A, Pelegrini-Issac M, Messe A, Vidailhet M, Lehericy S, Benali H (2012) Functional immaturity of cortico-basal ganglia networks in Gilles de la Tourette syndrome. Brain 135 (Pt 6):1937-1946. doi:10.1093/brain/aws056
12. Watts DJ, Strogatz SH (1998) Collective dynamics of 'small-world' networks. Nature 393 (6684):440-442
13. Salvador R, Suckling J, Coleman MR, Pickard JD, Menon D, Bullmore E (2005) Neurophysiological architecture of functional magnetic resonance images of human brain. Cereb Cortex 15 (9):1332-1342. doi:10.1093/cercor/bhi016
14. Wang J, Li T, Wang N, Xian J, He H (2016) Graph theoretical analysis reveals the reorganization of the brain network pattern in primary open angle glaucoma patients. European radiology. doi:10.1007/s00330-016-4221-x
15. Cerasa A, Castiglioni I, Salvatore C, Funaro A, Martino I, Alfano S, Donzuso G, Perrotta P, Gioia MC, Gilardi MC (2015) Biomarkers of eating disorders using support vector machine analysis of structural neuroimaging data: preliminary results. Behavioural neurology 51 (1):50-62
16. Liu F, Wee CY, Chen H, Shen D (2014) Inter-modality relationship constrained multi-modality multi-task feature selection for Alzheimer's Disease and mild cognitive impairment identification. Neuroimage 84:466-475. doi:10.1016/j.neuroimage.2013.09.015
17. Chi M, Guo S, Ning Y, Li J, Qi H, Gao M, Wang J, Hu X, Guo Y, Yang Y (2014) Using support vector machine to identify imaging biomarkers of major depressive disorder and anxious depression. Springer Berlin Heidelberg,
18. Dai D, Wang J, Hua J, He H (2012) Classification of ADHD children through multimodal Magnetic Resonance Imaging. Frontiers in Systems Neuroscience 6:63-63
19. Dai D, He H, Vogelstein JT, Hou Z (2013) Accurate prediction of AD patients using cortical thickness networks. Machine Vision & Applications 24 (7):1445-1457
20. Jie B, Zhang D, Gao W, Wang Q, Wee CY, Shen D (2014) Integration of network topological and connectivity properties for neuroimaging classification. IEEE transactions on bio-medical engineering 61 (2):576-589. doi:10.1109/TBME.2013.2284195
21. Jin Y, Wee CY, Shi F, Thung KH, Ni D, Yap PT, Shen D (2015) Identification of infants at high-risk for autism spectrum disorder using multiparameter multiscale white matter connectivity networks. Human brain mapping
22. Sacchet MD, Prasad G, Folandross LC, Thompson PM, Gotlib IH (2015) Support Vector Machine Classification of Major Depressive Disorder Using Diffusion-Weighted Neuroimaging and Graph Theory. Frontiers in psychiatry 6:21
23. Greene DJ, Church JA, Dosenbach NUF, Nielsen AN, Adeyemo B, Nardos B, Petersen SE, Black KJ, Schlaggar BL (2016) Multivariate pattern classification of pediatric Tourette syndrome using functional connectivity MRI. Developmental Science
24. Liao W, Yu Y, Miao H-H, Feng Y-X, Ji G-J, Feng J-H (2016) Inter-hemispheric Intrinsic Connectivity as a Neuromarker for the Diagnosis of Boys with Tourette Syndrome. Molecular neurobiology:1-9
25. Wen H, Liu Y, Wang J, Zhang J, Peng Y, He H A diagnosis model for early Tourette syndrome children

based on brain structural network characteristics. In: SPIE Medical Imaging, 2016. International Society for Optics and Photonics, pp 97852R-97852R-97859
26. Golden GS (1977) The effect of central nervous system stimulants on Tourette syndrome. Ann Neurol 2 (1):69–70
27. Scahill L, Riddle MA, McSwiggin-Hardin M, Ort SI, King RA, Goodman WK, Cicchetti D, Leckman JF (1997) Children's Yale-Brown Obsessive Compulsive Scale: reliability and validity. J Am Acad Child Adolesc Psychiatry 36 (6):844-852. doi:10.1097/00004583-199706000-00023
28. Retz-Junginger P, Retz W, Blocher D, Stieglitz RD, Georg T, Supprian T, Wender PH, Rosler M (2003) [Reliability and validity of the Wender-Utah-Rating-Scale short form. Retrospective assessment of symptoms for attention deficit/hyperactivity disorder]. Der Nervenarzt 74 (11):987-993. doi:10.1007/s00115-002-1447-4
29. Leckman JF, Riddle MA, Hardin MT, Ort SI, Swartz KL, Stevenson J, Cohen DJ (1989) The Yale Global Tic Severity Scale: initial testing of a clinician-rated scale of tic severity. J Am Acad Child Adolesc Psychiatry 28 (4):566-573. doi:10.1097/00004583-198907000-00015
30. Tzourio-Mazoyer N, Landeau B, Papathanassiou D, Crivello F, Etard O, Delcroix N, Mazoyer B, Joliot M (2002) Automated Anatomical Labeling of Activations in SPM Using a Macroscopic Anatomical Parcellation of the MNI MRI Single-Subject Brain. Neuroimage 15 (1):273-289
31. Cao Q, Shu N, An L, Wang P, Sun L, Xia MR, Wang JH, Gong GL, Zang YF, Wang YF, He Y (2013) Probabilistic diffusion tractography and graph theory analysis reveal abnormal white matter structural connectivity networks in drug-naive boys with attention deficit/hyperactivity disorder. J Neurosci 33 (26):10676-10687. doi:10.1523/JNEUROSCI.4793-12.2013
32. Wang J, Zuo X, He Y (2010) Graph-based network analysis of resting-state functional MRI. Front Syst Neurosci 4:16. doi:10.3389/fnsys.2010.00016
33. He Y, Dagher A, Chen Z, Charil A, Zijdenbos A, Worsley K, Evans A (2009) Impaired small-world efficiency in structural cortical networks in multiple sclerosis associated with white matter lesion load. Brain 132 (Pt 12):3366-3379. doi:10.1093/brain/awp089
34. Zhang J, Wang J, Wu Q, Kuang W, Huang X, He Y, Gong Q (2011) Disrupted brain connectivity networks in drug-naive, first-episode major depressive disorder. Biol Psychiatry 70 (4):334-342. doi:10.1016/j.biopsych.2011.05.018
35. Zhang D, Liu X, Chen J, Liu B, Wang J (2015) Widespread increase of functional connectivity in Parkinson's disease with tremor: a resting-state FMRI study. Frontiers in aging neuroscience 7:6. doi:10.3389/fnagi.2015.00006
36. Wang J, Wang X, Xia M, Liao X, Evans A, He Y (2015) GRETNA: a graph theoretical network analysis toolbox for imaging connectomics. Frontiers in human neuroscience 9:386. doi:10.3389/fnhum.2015.00386
37. Wang B, Mezlini AM, Demir F, Fiume M, Tu Z, Brudno M, Haibe-Kains B, Goldenberg A (2014) Similarity network fusion for aggregating data types on a genomic scale. Nature methods 11 (3):333-337. doi:10.1038/nmeth.2810
38. Guyon I, Weston J, Barnhill S, Vapnik V (2002) Gene selection for cancer classification using support vector machines. Mach Learn 46 (1-3):389-422. doi:Doi 10.1023/A:1012487302797
39. Wen H, Liu Y, Rekik I, Wang S, Chen Z, Zhang J, Zhang Y, Peng Y, He H (2017) Multi-modal multiple kernel learning for accurate identification of Tourette syndrome children. Pattern Recognition 63:601-611
40. Wilson SM, Ogar JM, Laluz V, Growdon M, Jang J, Glenn S, Miller BL, Weiner MW, Gorno-Tempini

ML (2009) Automated MRI-based classification of primary progressive aphasia variants. Neuroimage 47 (4):1558-1567. doi:10.1016/j.neuroimage.2009.05.085
41. Benjamini Y, Hochberg Y (2015) Controlling The False Discovery Rate - A Practical And Powerful Approach To Multiple Testing. Journal of the Royal Statistical Society 57 (57):289-300
42. Achard S, Salvador R, Whitcher B, Suckling J, Bullmore E (2006) A resilient, low-frequency, small-world human brain functional network with highly connected association cortical hubs. J Neurosci 26 (1):63-72. doi:10.1523/JNEUROSCI.3874-05.2006
43. He Y, Chen ZJ, Evans AC (2007) Small-world anatomical networks in the human brain revealed by cortical thickness from MRI. Cereb Cortex 17 (10):2407-2419. doi:10.1093/cercor/bhl149
44. Iturria-Medina Y, Sotero RC, Canales-Rodriguez EJ, Aleman-Gomez Y, Melie-Garcia L (2008) Studying the human brain anatomical network via diffusion-weighted MRI and Graph Theory. Neuroimage 40 (3):1064-1076. doi:10.1016/j.neuroimage.2007.10.060
45. Gong G, He Y, Concha L, Lebel C, Gross DW, Evans AC, Beaulieu C (2009) Mapping anatomical connectivity patterns of human cerebral cortex using in vivo diffusion tensor imaging tractography. Cereb Cortex 19 (3):524-536. doi:10.1093/cercor/bhn102
46. Liu T, Chen Y, Lin P, Wang J (2015) Small-World Brain Functional Networks in Children With Attention-Deficit/Hyperactivity Disorder Revealed by EEG Synchrony. Clinical EEG and neuroscience 46 (3):183-191. doi:10.1177/1550059414523959
47. Wang L, Zhu C, He Y, Zang Y, Cao Q, Zhang H, Zhong Q, Wang Y (2009) Altered small-world brain functional networks in children with attention-deficit/hyperactivity disorder. Human brain mapping 30 (2):638-649. doi:10.1002/hbm.20530
48. Latora V, Marchiori M (2001) Efficient behavior of small-world networks. Physical review letters 87 (19):198701. doi:10.1103/PhysRevLett.87.198701
49. Liu Y, Miao W, Wang J, Gao P, Yin G, Zhang L, Lv C, Ji Z, Yu T, Sabel BA, He H, Peng Y (2013) Structural abnormalities in early Tourette syndrome children: a combined voxel-based morphometry and tract-based spatial statistics study. Plos One 8 (9):e76105. doi:10.1371/journal.pone.0076105
50. Wen H, Liu Y, Wang J, Rekik I, Zhang J, Zhang Y, Tian H, Peng Y, He H (2016) Combining tract- and atlas-based analysis reveals microstructural abnormalities in early Tourette syndrome children. Human brain mapping 37 (5):1903-1919. doi:10.1002/hbm.23146
51. Liu Y, Duan YY, He Y, Wang J, Xia MR, Yu CS, Dong HQ, Ye J, Butzkueven H, Li KC, Shu N (2012) Altered Topological Organization of White Matter Structural Networks in Patients with Neuromyelitis Optica. Plos One 7 (11). doi:ARTN e48846
10.1371/journal.pone.0048846
52. Sporns O, Honey CJ, Kotter R (2007) Identification and classification of hubs in brain networks. Plos One 2 (10):e1049. doi:10.1371/journal.pone.0001049
53. WU J, QIAN Z, TAO L, DING S (2013) The Comparison of Orientation and Methods of Hubs in the Resting State Functional Brain Network. Journal of Biomedical Engineering Research 3:006
54. Tang Y, Long J, Wang W, Liao J, Xie H, Zhao G, Zhang H (2016) Aberrant functional brain connectome in people with antisocial personality disorder. Sci Rep 6:26209. doi:10.1038/srep26209
55. De Asis-Cruz J, Bouyssi-Kobar M, Evangelou I, Vezina G, Limperopoulos C (2015) Functional properties of resting state networks in healthy full-term newborns. Sci Rep 5:17755. doi:10.1038/srep17755
56. Yuan W, Wade SL, Babcock L (2015) Structural connectivity abnormality in children with acute mild traumatic brain injury using graph theoretical analysis. Human brain mapping 36 (2):779-792.

doi:10.1002/hbm.22664
57. Worbe Y, Marrakchi-Kacem L, Lecomte S, Valabregue R, Poupon F, Guevara P, Tucholka A, Mangin JF, Vidailhet M, Lehericy S, Hartmann A, Poupon C (2015) Altered structural connectivity of cortico-striato-pallido-thalamic networks in Gilles de la Tourette syndrome. Brain 138 (Pt 2):472-482. doi:10.1093/brain/awu311
58. Tinaz S, Belluscio BA, Malone P, Veen JWVD, Hallett M, Horovitz SG (2014) Role of the sensorimotor cortex in Tourette syndrome using multimodal imaging. Human brain mapping 35 (12):5834-5846
59. Ludolph AG, Juengling FD, Libal G, Ludolph AC, Fegert JM, Kassubek J (2006) Grey-matter abnormalities in boys with Tourette syndrome: magnetic resonance imaging study using optimised voxel-based morphometry. The British journal of psychiatry : the journal of mental science 188:484-485. doi:10.1192/bjp.bp.105.008813
60. Worbe Y, Gerardin E, Hartmann A, Valabrégue R, Chupin M, Tremblay L, Vidailhet M, Colliot O, Lehéricy S (2010) Distinct structural changes underpin clinical phenotypes in patients with Gilles de la Tourette syndrome. Brain 133 (Pt 12):3649-3660
61. Gates L, Clarke JA, Somorjai R, Jarmasz M, Vandorpe R, Dursun SM (2004) Neuroanatomy of coprolalia in Tourette syndrome using functional magnetic resonance imaging. Progress in Neuro-Psychopharmacology and Biological Psychiatry 28 (2):397-400
62. Thomalla G, Jonas M, Baumer T, Siebner HR, Biermann-Ruben K, Ganos C, Orth M, Hummel FC, Gerloff C, Muller-Vahl K, Schnitzler A, Munchau A (2014) Costs of control: decreased motor cortex engagement during a Go/NoGo task in Tourette's syndrome. Brain 137 (Pt 1):122-136. doi:10.1093/brain/awt288
63. Buse J, Beste C, Herrmann E, Roessner V (2015) Neural correlates of altered sensorimotor gating in boys with Tourette Syndrome: A combined EMG/fMRI study. The world journal of biological psychiatry : the official journal of the World Federation of Societies of Biological Psychiatry:1-11. doi:10.3109/15622975.2015.1112033
64. Bohlhalter S, Goldfine A, Matteson S, Garraux G, Hanakawa T, Kansaku K, Wurzman R, Hallett M (2006) Neural correlates of tic generation in Tourette syndrome: an event-related functional MRI study. Brain 129 (Pt 8):2029-2037. doi:10.1093/brain/awl050
65. Zapparoli L, Porta M, Paulesu E (2015) The anarchic brain in action: the contribution of task-based fMRI studies to the understanding of Gilles de la Tourette syndrome. Curr Opin Neurol 28 (6):604-611. doi:10.1097/WCO.0000000000000261
66. Roessner V, Overlack S, Schmidt-Samoa C, Baudewig J, Dechent P, Rothenberger A, Helms G (2011) Increased putamen and callosal motor subregion in treatment-naive boys with Tourette syndrome indicates changes in the bihemispheric motor network. Journal of child psychology and psychiatry, and allied disciplines 52 (3):306-314. doi:10.1111/j.1469-7610.2010.02324.x
67. Stern E, Silbersweig DA, Chee KY, Holmes A, Robertson MM, Trimble M, Frith CD, Frackowiak RS, Dolan RJ (2000) A functional neuroanatomy of tics in Tourette syndrome. Archives of general psychiatry 57 (8):741-748
68. Tinaz S, Belluscio BA, Malone P, Veen JW, Hallett M, Horovitz SG (2014) Role of the sensorimotor cortex in Tourette syndrome using multimodal imaging. Human brain mapping 35 (12):5834-5846
69. Felling RJ, Singer HS (2011) Neurobiology of tourette syndrome: current status and need for further investigation. Journal of Neuroscience the Official Journal of the Society for Neuroscience 31 (35):12387-12395

70. Robertson MM (2000) Tourette syndrome, associated conditions and the complexities of treatment. Brain 123:425-462. doi:DOI 10.1093/brain/123.3.425

Figure Legends

Figure 1. The flowchart for constructing the FC networks of different thresholds using rs-fMRI data.

Figure 2. The flowchart of our proposed classification framework, including the multi-threshold similarity network fusion and subsequent TS classification. Of note, when the network construction and subsequent graph theory analysis were implemented using *GRETNA* toolbox, we considered the full network (composed of both positive correlations and the absolute values of the negative correlations) [36], thus, the resultant connection strengths range from 0 to 1.

Figure 3. The flow chart of the nested CV procedure in our classification framework.

Figure 4. Between-group differences in topological properties of functional connectivity networks. Asterisk (*) donates significant difference ($p<0.05$) between groups at corresponding sparsity threshold. Compared with control group, TS group has significantly decreased network strength, global, local efficiency, clustering coefficient (C_p), and increased shortest path length (L_p), γ, λ and σ in the FC networks over a wide range of thresholds.

Figure 5. Distribution of hub regions in the WM structural networks of the control and TS groups and nodes with significant differences in TS children. (A, B) 3D representations of the hub distributions in the healthy control (HC) and TS groups, respectively. The hub nodes are shown in blue and red with node sizes indicating their nodal betweenness centrality values. (C) The disrupted nodes with the significantly decreased or increased nodal betweenness centrality in TS group are shown in red or blue, and the node sizes indicate the t values in t-test. The brain graphs were visualized by using BrainNet Viewer software (http://www.nitrc.org/projects/bnv/). For the abbreviations of nodes, see Table 1.

Figure 6. Pearson correlations between nodal topological properties and clinical variables. (A) Both significantly positive or negatively correlations ($p<0.05$) between YGTSS and nodal betweenness centrality were found. (B) Significantly positive correlation ($p<0.05$) between tics duration and nodal betweenness centrality.

Figure 7. Original networks and fused networks of three randomly selected healthy children and TS children, respectively.

Figure 8. Results of TS classification based on multi-threshold fused FC networks. (A) The overall ROC curves for 20 times of nested CV, which demonstrate the superior performance of our framework over other comparison methods. The overall ROC curves were generated by concatenating the estimated probability matrix of each subject in each group across 20 rounds of nested CV. (B) The brain regions with most discriminative nodal topological properties for classification. The brain graphs were visualized by *volume to surface* function in BrainNet Viewer software. The regional colors with progressive shade (from blue to red) indicate the frequency of being selected by the nested CV procedure. Abbreviation is the same as Table 3.

Table 1. Demographics and clinical characteristics of the TS participants. Abbreviations: + = present, − = absent; YGTSS = Yale Global Tic Severity Scale; M = male; F = female

ID	sex	age(y)	YGTSS	Duration	OCD	Motor tics		Vocal tics	
						Simple	Complex	Simple	Complex
1	M	5	36	0.17	No	+	+	-	-
2	F	12	52	4	No	+	+	+	-
3	M	14	65	1.5	No	+	+	+	+
4	M	6	23	0.25	No	+	+	-	-
5	M	10	80	2	No	+	+	+	-
6	M	6	50	0.67	No	+	+	-	-
7	M	8	44	2	No	+	+	+	-
8	M	12	30	2	No	+	+	-	-
9	M	10	24	4	No	+	+	-	-
10	M	12	25	1	No	+	+	-	-
11	F	6	52	0.25	No	+	+	+	-
12	M	11	30	1.2	No	+	+	-	-
13	F	8	10	0.625	No	+	+	-	-
14	M	3	38	0.17	No	+	+	+	-
15	M	5	58	1	No	+	+	+	-
16	F	8	42	3	No	+	+	+	-
17	M	11	30	3	No	+	+	+	-
18	M	7	52	0.17	No	+	+	+	-
19	M	12	79	6	No	+	+	+	+
20	M	13	51	2	No	+	+	+	-
21	M	11	24	1	No	+	+	-	-
22	M	9	55	1.75	No	+	+	+	-
23	F	13	76	1.5	No	+	+	+	-
24	M	4	35	0.42	No	+	+	-	-
25	M	10	35	1	No	+	+	+	-
26	M	11	32	0.917	No	+	+	-	-
27	M	7	59	2.3	No	+	+	+	-
28	M	6	42	2.5	No	+	+	+	-
29	F	4	66	0.25	No	+	+	+	-

Table 2. The 116 cortical and subcortical regions of interest defined in our study.

Regions	Abbr.	Regions	Abbr.
Precentral gyrus	PreCG	Lingual gyrus	LING
Superior frontal gyrus, dorsolateral	SFGdor	Superior occipital gyrus	SOG
Superior frontal gyrus, orbital part	ORBsup	Middle occipital gyrus	MOG
Middle frontal gyrus	MFG	Inferior occipital gyrus	IOG
Middle frontal gyrus orbital part	ORBmid	Fusiform gyrus	FFG
Inferior frontal gyrus, opercular part	IFGoperc	Postcentral gyrus	PoCG
Inferior frontal gyrus, triangular part	IFGtriang	Superior parietal gyrus	SPG
Inferior frontal gyrus, orbital part	ORBinf	Inferior parietal, but supramarginal and angular gyri	IPL
Rolandic operculum	ROL	Supramarginal gyrus	SMG
Supplementary motor area	SMA	Angular gyrus	ANG
Olfactory cortex	OLF	Precuneus	PCUN
Superior frontal gyrus, medial	SFGmed	Paracentral lobule	PCL
Superior frontal gyrus, medial orbital	ORBsupmed	Caudate nucleus	CAU
Gyrus rectus	REC	Lenticular nucleus, putamen	PUT
Insula	INS	Lenticular nucleus, pallidum	PAL
Anterior cingulate and paracingulate gyri	ACG	Thalamus	THA
Median cingulate and paracingulate gyri	DCG	Heschl gyrus	HES
Posterior cingulate gyrus	PCG	Superior temporal gyrus	STG
Hippocampus	HIP	Temporal pole: superior temporal gyrus	TPOsup
Parahippocampal gyrus	PHG	Middle temporal gyrus	MTG
Amygdala	AMYG	Temporal pole: middle temporal gyrus	TPOmid
Calcarine fissure and surrounding cortex	CAL	Inferior temporal gyrus	ITG
Cuneus	CUN		

Due to space limitations, the detailed descriptions and abbreviations of 26 cerebellum regions could be found on (http://neuro.imm.dtu.dk/wiki/Automated_Anatomical_Labeling).

Table 3. Global and local topological properties used in the study.

Global network properties	
Network strength S_p	S_p is the strength of the network, which is defined as the mean degree of all the regions in the brain network.
Global Efficiency E_{glob}	E_{glob} is defined as the mean value of all regions' global efficiency.
Local Efficiency E_{loc}	E_{loc} is defined as the mean value of all regions' local efficiency.
Shortest path length L_p	L_p is defined as the average length of the shortest path between every. two nodes in network G, which quantifies the ability for information to be propagated in parallel.
Clustering coefficient C_p	C_p is the average clustering coefficient over all nodes, which indicates the extent of local interconnectivity or cliquishness in a network
Normalized L_p (λ)	$\lambda=L_p^{real}/ L_p^{rand}$, L_p^{rand} is the mean shortest path length of 100 matched random networks.
Normalized C_p (γ)	$\gamma= C_p^{real}/ C_p^{rand}$, C_p^{rand} is the mean clustering coefficient of 100 matched random networks.
Small-worldness σ	$\sigma=\lambda/\gamma$, A real network would be considered small world if $\gamma>1$ and $\lambda\approx1$.
Local nodal properties	
Nodal Betweenness Centrality $B_{nodal}(i)$	$B_{nodal}(i)$ is defined as the fraction of all shortest paths in the network G that pass through a given node i, The mathematical definition is presented in (1).

Table 4. Group comparisons of AUC values (mean ± SD) of global network properties.

	S_p	E_{glob}	E_{loc}	L_p	C_p	λ	γ	σ
HC	11.81±2.64	0.19±0.03	0.26±0.05	1.49±0.22	0.21±0.05	0.58±0.02	0.73±0.1	0.64±0.09
TS	9.5±2.26	0.16±0.03	0.21±0.04	1.71±0.22	0.16±0.05	0.59±0.01	0.81±0.09	0.71±0.07
p	<0.001*	<0.001*	<0.001*	<0.001*	<0.001*	0.409	0.001*	0.002*

Two-sample t-tests were used to determine the between-group differences, all the significant p values (<0.05) were derived after FDR correction for multiple comparison.

Table 5. Hub regions of FC networks in control and TS groups. B_{nodal} represents the AUC value of the nodal betweenness centrality across thresholds.

HC			**TS**		
Hub regions	Category	mean B_{nodal}	**Hub regions**	Category	mean B_{nodal}
PreCG.L	Frontal	43.080	**PreCG.L**	Frontal	39.929
PreCG.R	Frontal	47.068	**SFGdor.R**	Frontal	62.137
SFGdor.L	Frontal	41.663	**MFG.R**	Frontal	43.978
SFGdor.R	Frontal	51.061	**DCG.L**	Cingulate	39.690
DCG.L	Cingulate	48.844	**PHG.R**	Temporal	59.098
DCG.R	Cingulate	58.951	**PCUN.L**	Parietal	43.211
PHG.R	Temporal	56.168	**PCUN.R**	Parietal	43.387
PCUN.L	Parietal	45.605	**STG.R**	Temporal	49.713
STG.R	Temporal	51.973	**TPOsup.R**	Temporal	48.596
MTG.L	Temporal	39.988	**ITG.R**	Temporal	58.980
MTG.R	Temporal	43.550			
ITG.R	Temporal	55.685			

Table 6. Brain regions with significant between-group differences in nodal betweenness centrality. B_{nodal} represents the AUC values (mean ± SD) of the nodal betweenness centrality of each group.

		B_{nodal}			
Category	Region	HC	TS	t value	p value
Frontal	ORBsup.L	27.49±23.24	17.55±12.81	2.066	0.043
	ORBinf.R	19.69±20.68	37.15±34.82	-2.535	0.014
	PCL.R	9.77±10.43	18.61±18.74	-2.43	0.018
Insula	INS.R	12.92±13.55	27.37±24.59	-3.038	0.003
Cingulate	DCG.R	58.95±44.27	34.88±27.4	2.565	0.013
Temporal	HIP.R	17.16±21.06	30.63±23.3	-2.461	0.017
	FFG.R	15.81±15.49	27.25±20.07	-2.614	0.011
Occipital	LING.R	29.49±36.38	14.44±15.75	2.078	0.042
	MOG.R	12.96±14.97	23.52±15.11	-2.831	0.006
Parietal	IPL.R	12.98±14.15	22.9±18.77	-2.451	0.017
	ANG.L	7.64±9.74	16.61±22.67	-2.168	0.034
	ANG.R	10.11±11.83	22.87±23.19	-2.903	0.005
Central	PAL.L	11.35±15.79	5.4±4.07	1.977	0.033

Table 7. Classification performances (mean ± SD) of all methods in percentage.

Feature	ACC(%)	SEN(%)	SPE(%)	AUC(%)
Original FC	72.73±2.40	73.10±5.67	72.43±2.26	76.22±4.36
No Threshold	74.55±2.25	74.48±1.89	74.59±4.10	83.56±1.28
Single Threshold	76.97±1.66	74.48±5.77	78.92±2.26	84.36±3.93
Fused Network	**88.79±2.33**	**88.45±4.23**	**89.05±3.60**	**94.96±2.43**

We ran nested CV twenty times, and then calculated mean ± standard deviation (SD).

Table 8. The top 29 discriminative network features selected by the nested CV method as the most salient for TS classification.

Region	Feature	Num	Rate
Right fusiform gyrus	BC	200	100.0%
Left superior parietal gyrus	BC	200	100.0%
Left hippocampus	BC	198	99.0%
Left rolandic operculum	BC	197	98.5%
Right paracentral lobule	BC	197	98.5%
Right inferior frontal gyrus, orbital part	BC	197	98.5%
Left middle frontal gyrus, orbital part	BC	196	98.0%
Right hippocampus	BC	196	98.0%
Left superior frontal gyrus, dorsolateral	BC	195	97.5%
Right heschl gyrus	BC	194	97.0%
Right lingual gyrus	BC	193	96.5%
Global topological property	γ	192	96.0%
Left middle occipital gyrus	BC	190	95.0%
Right putamen	BC	188	94.0%
Left heschl gyrus	BC	184	92.0%
Global topological property	L_p	184	92.0%
Global topological property	C_p	170	85.0%
Right rolandic operculum	BC	169	84.5%
Right middle temporal gyrus	BC	167	83.5%
Left caudate nucleus	BC	164	82.0%
Right posterior cingulate gyrus	BC	154	77.0%
Left postcentral gyrus	BC	152	76.0%
Right superior parietal gyrus	BC	134	67.0%
Left cuneus	BC	133	66.5%
Global topological property	E_{glob}	112	56.0%
Right superior temporal gyrus	BC	111	55.5%
Left middle frontal gyrus	BC	109	54.5%
Left fusiform gyrus	BC	101	50.5%
Global topological property	E_{loc}	101	50.5%

Num: the counts of each feature selected by our proposed method over the 20 rounds nested 10-fold CV. Rate: the frequency of being selected equals to Num/total times in 20 rounds nested 10-fold CV (200 times). +/-: parameter is increased/decreased in TS group compared to control group. P: p-value of two sample t-test. N.S.: parameter is not significantly different between both groups.

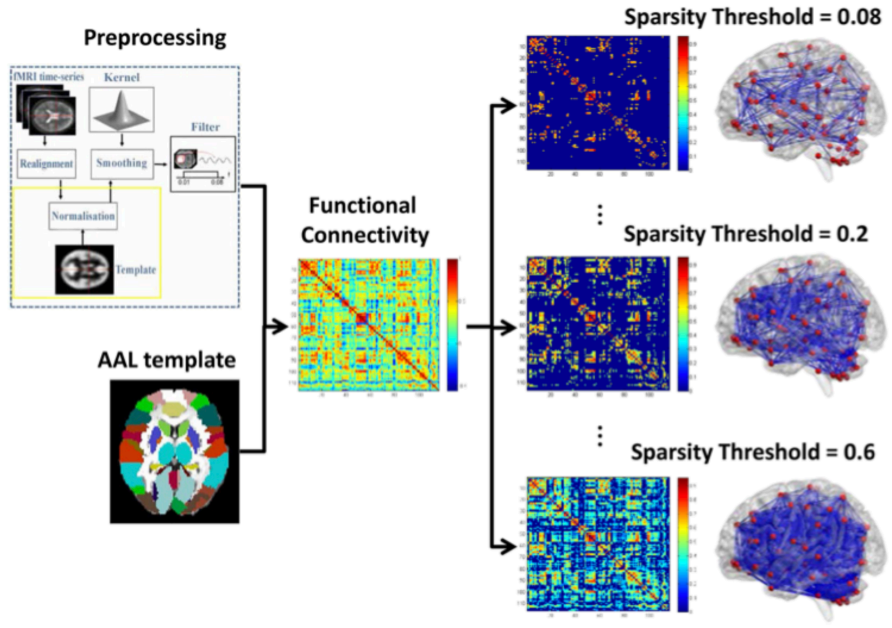

Fig.1 The flowchart for constructing the FC networks of different thresholds using rs-fMRI data

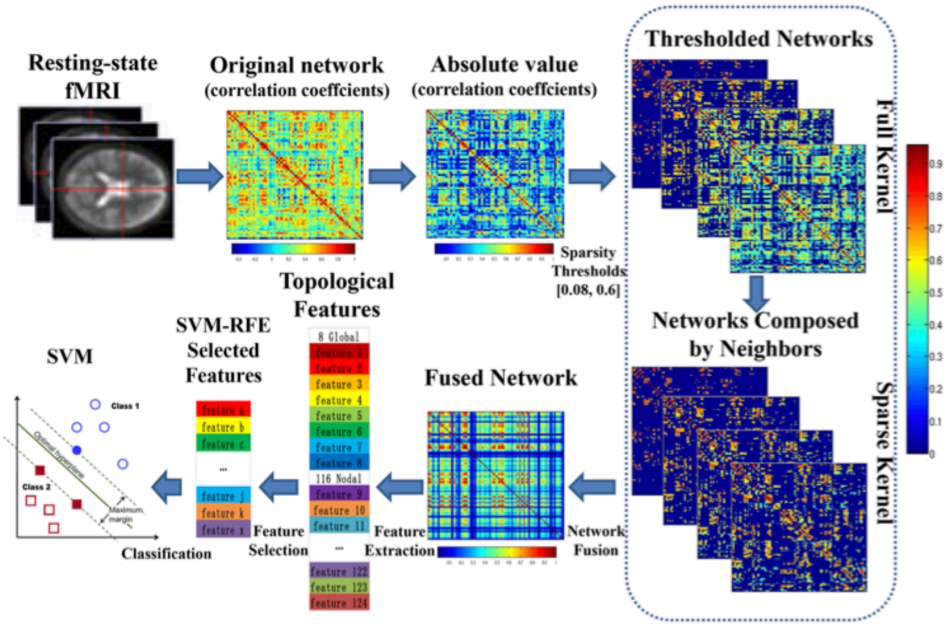

Fig.2 The flowchart of our proposed classification framework, including the multi-threshold similarity network fusion and subsequent TS classification. Of note, when the network construction and subsequent graph theory analysis were implemented using GRETNA toolbox, we considered the full network (composed of both positive correlations and the absolute values of the negative correlations) [36]; thus, the resultant connection strengths range from 0 to 1.

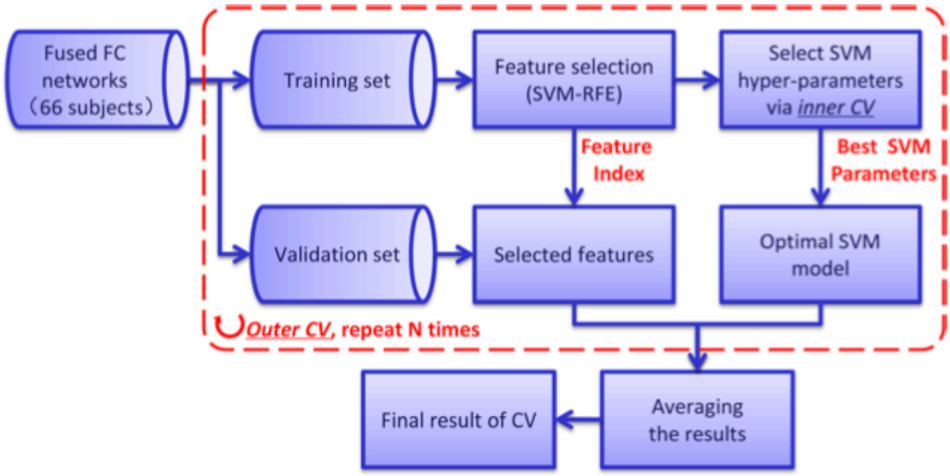

Fig.3 The flowchart of the nested CV procedure in our classification framework

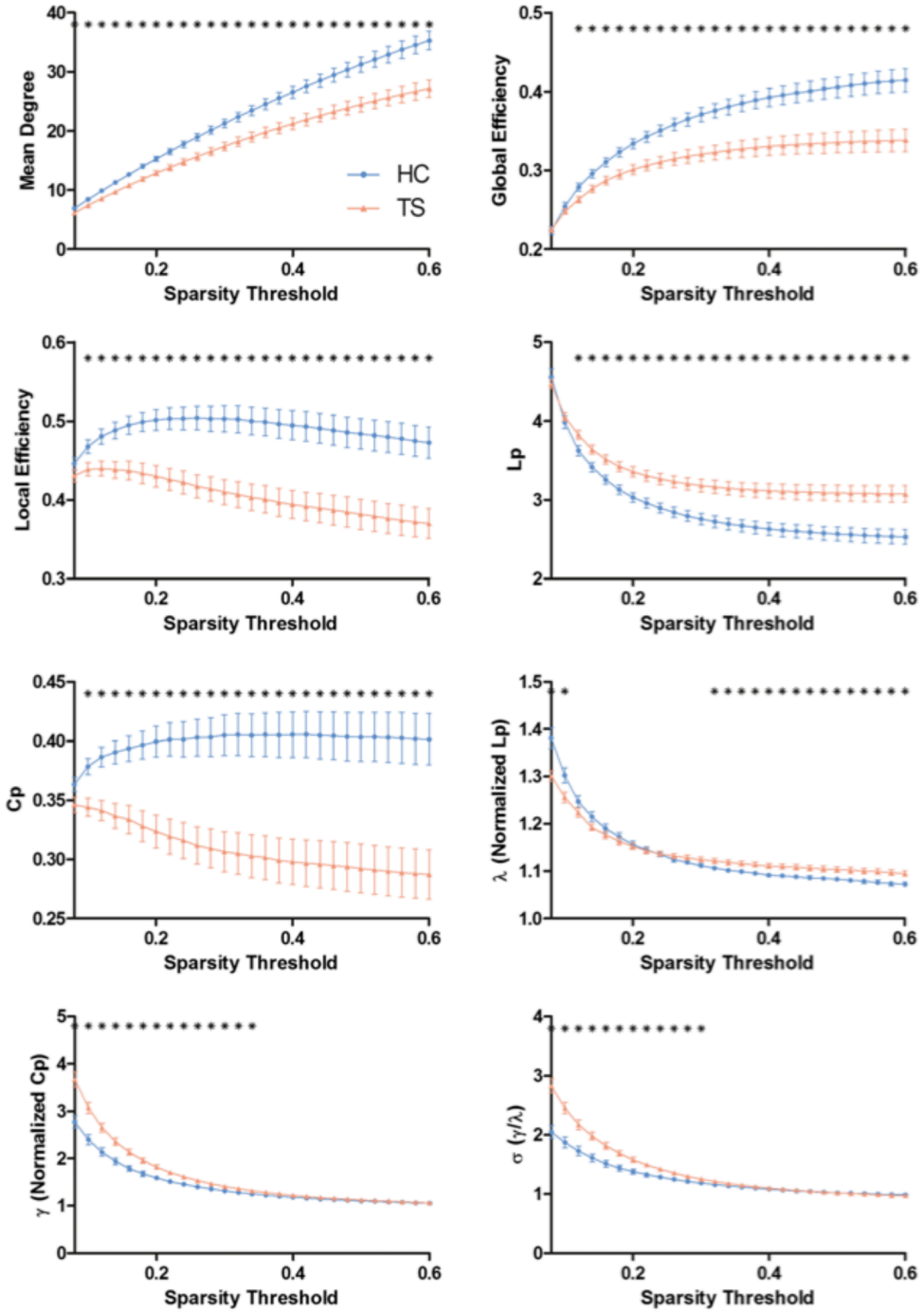

Fig.4 Between-group differences in topological properties of functional connectivity networks. Asterisk denotes significant difference ($p < 0.05$) between groups at corresponding sparsity threshold. Compared with control group, TS group has significantly decreased network strength, global, local efficiency, clustering coefficient (C_p), and increased shortest path length (L_p), γ, λ, and σ in the FC networks over a wide range of thresholds.

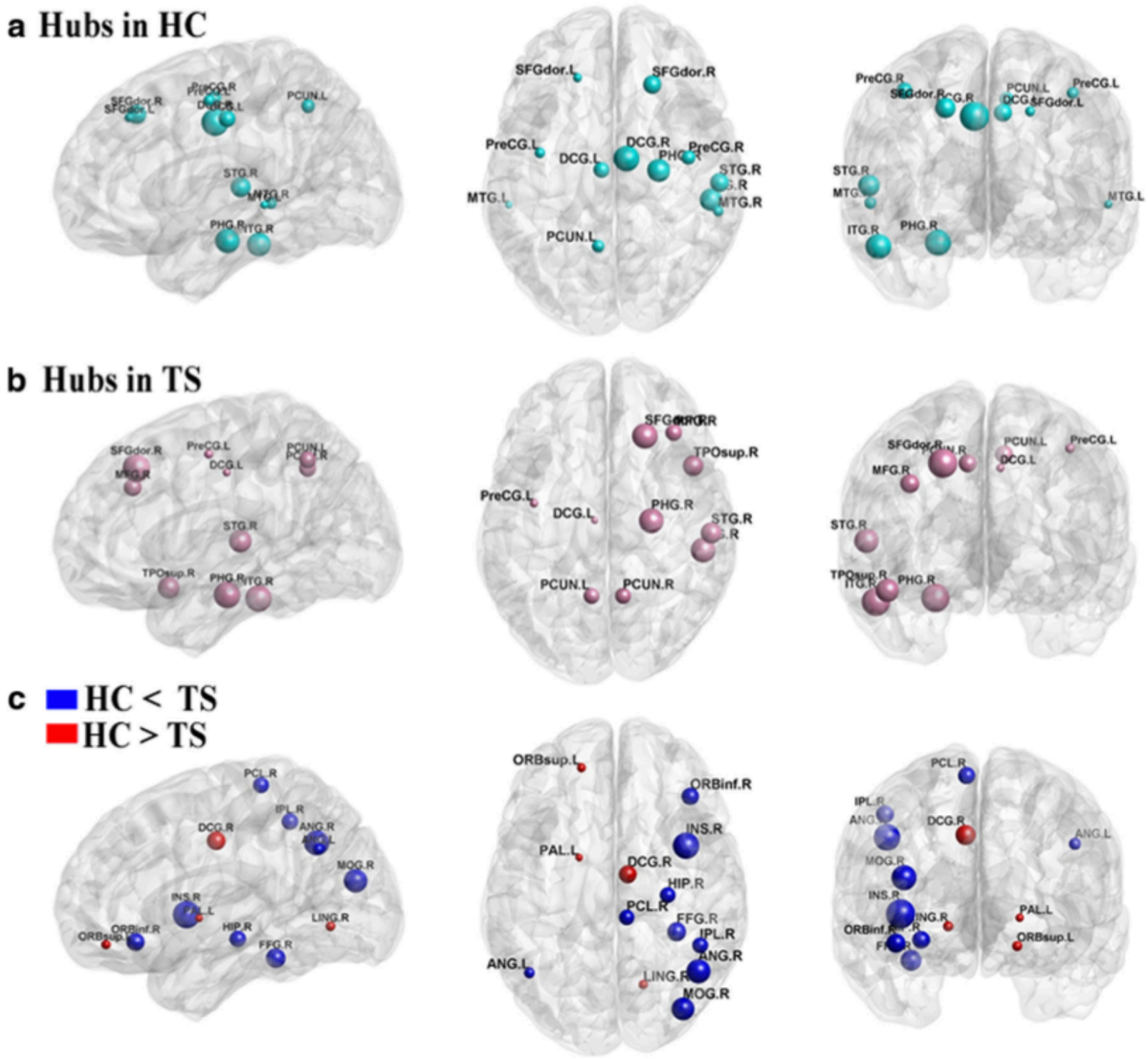

Fig.5 Distribution of hub regions in the WM structural networks of the control and TS groups and nodes with significant differences in TS children. a, b Three-dimensional representations of the hub distributions in the healthy control (HC) and TS groups, respectively. The hub nodes are shown in blue and red with node sizes indicating their nodal betweenness centrality values. c The disrupted nodes with the significantly decreased or increased nodal betweenness centrality in TS group are shown in red or blue, and the node sizes indicate the t values in t-test. The brain graphs were visualized by using BrainNet Viewer software (http://www.nitrc.org/projects/bnv/). For the abbreviations of nodes, see Table 1.

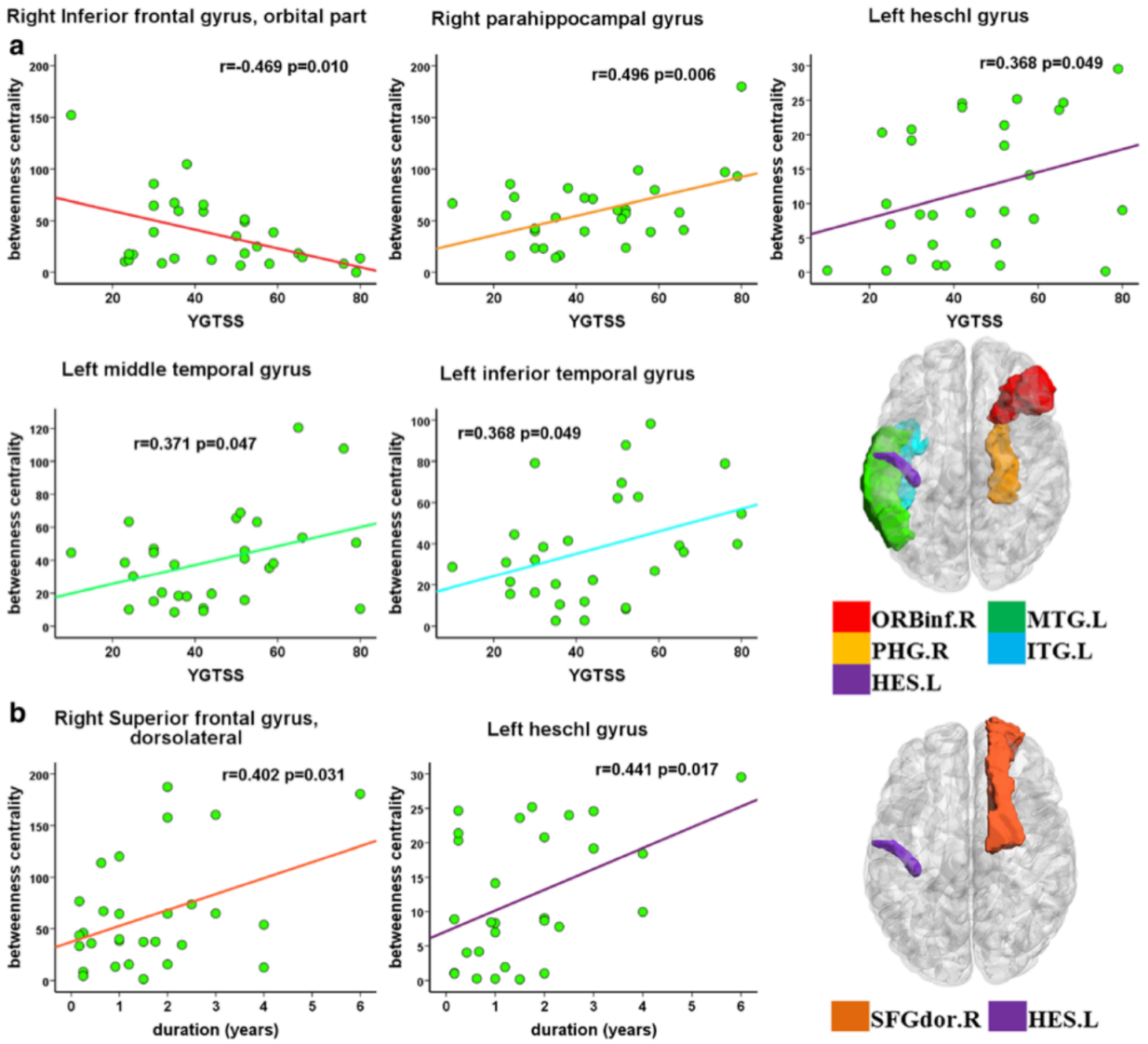

Fig.6 Partial correlations between nodal topological properties and clinical variables, using age and gender as covariates. a Both significantly positive or negatively correlations ($p < 0.05$) between YGTSS and nodal betweenness centrality were found. b Significantly positive correlation ($p < 0.05$) between tics duration and nodal betweenness centrality.

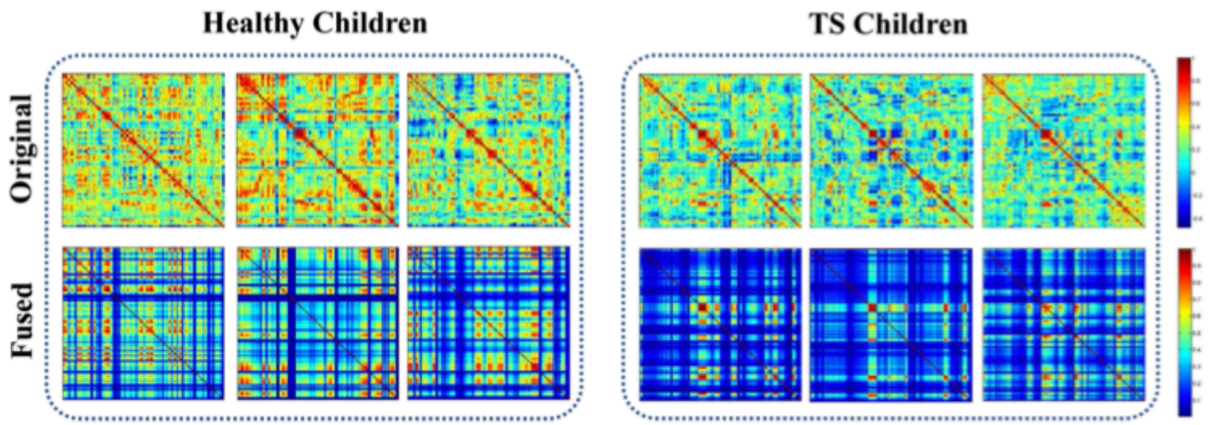

Fig. 7 Origina lnetworks and fused networks of three randomly selected healthy children and TS children, respectively.

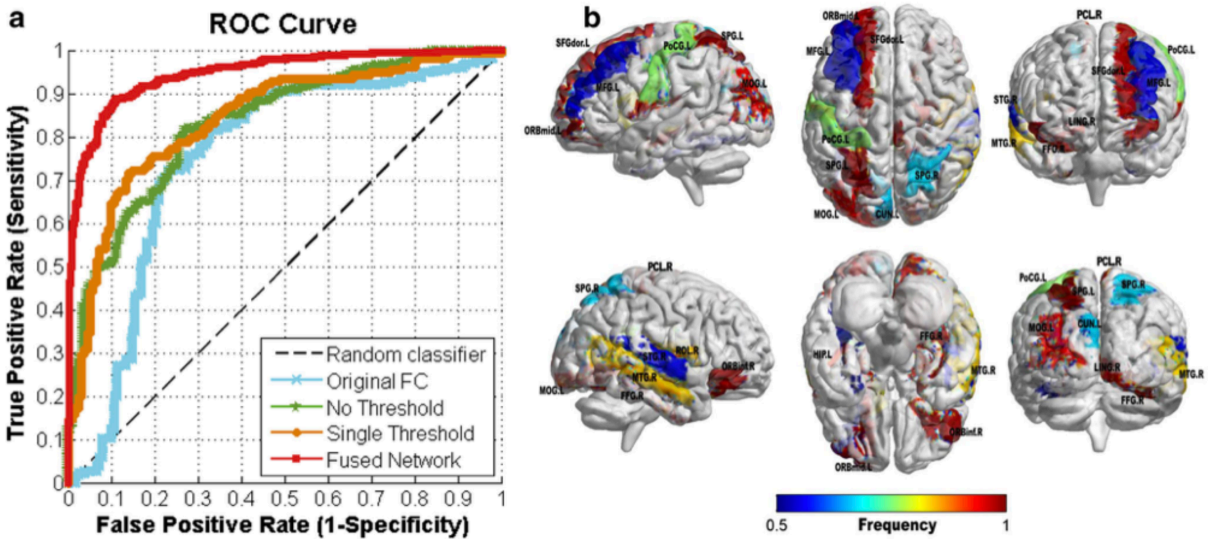

Fig.8 Results of TS classification based on multi-threshold fused FC networks. a The overall ROC curves for 20 times of nested CV, which demonstrate the superior performance of our framework over other comparison methods. The overall ROC curves were generated by concatenating the estimated probability matrix of each subject in each group across 20 rounds of nested CV. b The brain regions with most discriminative nodal topological properties for classification. The brain graphs were visualized by volume to surface function in BrainNet Viewer software. The regional colors with progressive shade (from blue to red) indicate the frequency of being selected by the nested CV procedure. Abbreviation is the same as Table 3.